energies

MDPI

Article

A Sparse Representation-Based Reconstruction Method of Electrical Impedance Imaging for Grounding Grid

Ke Zhu, Donghui Luo *, Zhengzheng Fu, Zhihang Xue and Xianghang Bu

State Grid Sichuan Electric Power Research Institute, Chengdu 610041, China; kez04@163.com (K.Z.); cathygold@foxmail.com (Z.F.); zhihangxue2024@163.com (Z.X.); xianghangbu2024@163.com (X.B.)
* Correspondence: dhluo@foxmail.com

Abstract: As a non-invasive imaging method, electrical impedance tomography (EIT) technology has become a research focus for grounding grid corrosion diagnosis. However, the existing algorithms have not produced ideal image reconstruction results. This article proposes an electrical impedance imaging method based on sparse representation, which can improve the accuracy of reconstructed images obviously. First, the basic principles of EIT are outlined, and the limitations of existing reconstruction methods are analyzed. Then, an EIT reconstruction algorithm based on sparse representation is proposed to address these limitations. It constructs constraints using the sparsity of conductivity distribution under a certain sparse basis and utilizes the accelerated Fast Iterative Shrinkage Threshold Algorithm (FISTA) for iterative solutions, aiming to improve the imaging quality and reconstruction accuracy. Finally, the grounding grid model is established by COMSOL simulation software to obtain voltage data, and the reconstruction effects of the Tikhonov regularization algorithm, the total variation regularization algorithm (TV), the one-step Newton algorithm (NOSER), and the sparse reconstruction algorithm proposed in this article are compared in MATLAB. The voltage relative error is introduced to evaluate the reconstructed image. The results show that the reconstruction algorithm based on sparse representation is superior to other methods in terms of reconstruction error and image quality. The relative error of the grounding grid reconstructed image is reduced by an average of 12.54%.

Keywords: electrical impedance imaging; sparse representation; grounding grid; finite element analysis; EIT reconstruction algorithm

check for updates

Citation: Zhu, K.; Luo, D.; Fu, Z.; Xue, Z.; Bu, X. A Sparse Representation-Based Reconstruction Method of Electrical Impedance Imaging for Grounding Grid. *Energies* **2024**, *17*, 6459. https://doi.org/10.3390/en17246459

Academic Editor: Tek Tjing Lie

Received: 18 November 2024
Revised: 12 December 2024
Accepted: 20 December 2024
Published: 22 December 2024

Copyright: © 2024 by the authors. Licensee MDPI, Basel, Switzerland. This article is an open access article distributed under the terms and conditions of the Creative Commons Attribution (CC BY) license (https://creativecommons.org/licenses/by/4.0/).

1. Introduction

Grounding is always highly valued by the operation and inspection departments as it is an important part of substations, power plants, and other power facilities [1]. It plays a crucial role in draining current and reducing step voltage, which ensures the personal safety of on-site staff and the normal operation of equipment. However, the grounding grids, mostly made of galvanized steel materials, tend to corrode over time in the soil. This corrosion can lead to thinning and, in severe cases, even fractures, resulting in a decline in grounding performance and posing a direct threat to personnel and equipment safety [2].

As power grid scale expands, the number of old substations also increases each year, and the grounding grids of these old substations are facing varying degrees of corrosion issues. Currently, the common approach is to periodically excavate and test the grounding grids (typically every 5 years) to assess their corrosion status [3]. However, there are some shortcomings for this method. The long excavation cycle is prone to evaluation gaps. The excavation for large substations is costly. Existing non-excavation detection methods such as the electrical network method and electrochemical method have great limitations due to the loss of design drawings and interference from complex natural environments.

Yan Xiaoheng and others proposed a grounding grid impedance imaging method based on the optimized differential multigrid–homotopy (MG-HT) algorithm and verified that it is better than the Tikhonov and HT algorithm in overcoming the pathological nature of the inverse problem of grounding grid impedance imaging [4]. Huang Zhicheng and others used laser-induced breakdown spectroscopy (LIBS) to measure the corrosion degree of grounding grids. Spectral data were collected from samples with different corrosion degrees, and the local outlier factor (LOF) algorithm was used to remove outliers, verifying the effectiveness and reliability of combining LIBS with machine learning to predict grounding grid corrosion [5].

In general, the main methods used for grounding grid fault diagnosis are the electrical network method and electromagnetic method [6]. It needs to know the topology of the grounding grid when adopting the electrical network method; this is difficult for substations whose grounding grid drawings is lost. In addition, it will lead to misdiagnosis when the structure of grounding grid is complex. For the electromagnetic method, the electromagnetic environment of substation is usually complex. This would cause big interference to the detection results.

Electrical impedance tomography (EIT) has the advantages of being non-invasive, having a simple structure, being easy to operate, and being low in cost [7]. It has broad application prospects. However, due to the limited number of nodes connected to the grounding grid, the existence of "soft field effect", and the complexity of its inverse problem, the difficulty of solving EIT is greatly increased. The effect of reconstructed image is usually poor.

Therefore, this article aims to solve the electrical impedance imaging problem of grounding grid based on sparse representation theory. It is expected to achieve accurate corrosion localization and corrosion degree diagnosis for substation grounding grid.

2. Principle of Fault Diagnosis

In electrical impedance imaging, current is injected into the conductors of grounding grid in turn, and the voltages between other conductors are then measured. Impedance changes of the corroded branches will be reflected in measured voltages. All the voltage data can be used to reconstruct an image to visualize the impedance distribution of the grounding grid and to identify corroded branches. The schematic diagram of the corrosion diagnosis by EIT technology is shown in Figure 1.

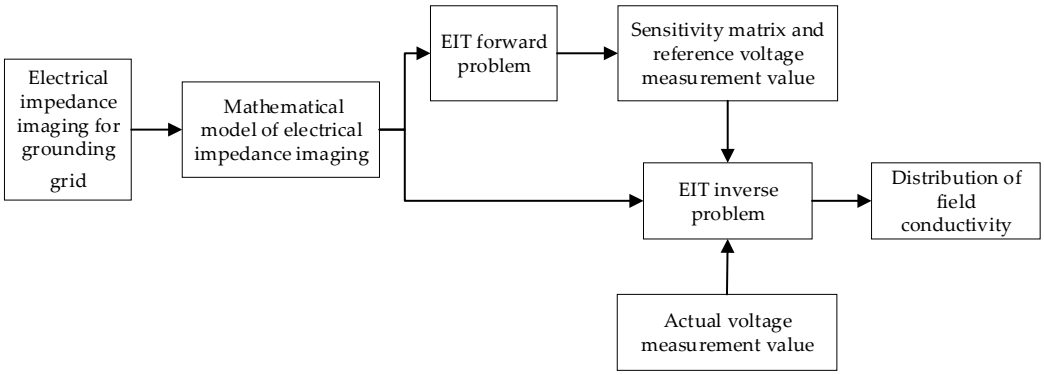

Figure 1. Schematic diagram of the corrosion diagnosis by EIT technology.

The mathematical problem of electrical impedance imaging is divided into two parts: the EIT forward problem and the EIT inverse problem [8]. The forward problem refers to calculating and determining the potential distribution in the field given conductivity distribution and injected current [9]. This process is relatively simple, similar to solving voltage through resistance and current. In contrast, the inverse problem is more complex and challenging [10]. It requires inferring conductivity distribution inside the field given injected current and some boundary potential distribution information [11].

Solving inverse problems is difficult because inverting complex internal physical properties from limited and possibly incomplete boundary information usually leads to multiple possible solutions [12]. However, in practical applications, we need a clear and reliable conductivity distribution solution to guide decision making or analysis. Therefore, the solution of the inverse problem requires specific algorithms and techniques to ensure uniqueness and accuracy.

The inverse problem solving process, also known as image reconstruction, is the key of the entire EIT technology [13]. It relies on advanced mathematical models, optimization algorithms, and numerical methods. Typical ones are regularization techniques and iterative solvers [14]. They are used to extract the conductivity information inside the field from limited measurement data, thereby achieving non-invasive imaging of the internal structure [15]. This process requires not only the efficiency and accuracy of the algorithm but also the effective dealing of factors such as measurement errors and noise interference [16].

2.1. EIT Forward Problem

The finite element method (FEM) decomposes the calculation area into multiple mesh elements, such as triangles, quadrilaterals, etc. This article discretizes them into triangular units, and then uses the node coordinate information of the triangle to solve the interpolation points of the function. Finally, the linear expression is solved by an equivalent variation theory. In the case of solving the measured voltage when the conductivity distribution of the grounding grid is known, the boundary problem of electrical impedance imaging can be written as follows according to the decomposition and boundary conditions:

$$\begin{aligned} F(\varphi) &= \frac{1}{2}\int_{\Omega}\sigma\left(\left(\frac{\partial\varphi}{\partial x}\right)^2+\left(\frac{\partial\varphi}{\partial y}\right)^2\right)dxdy \\ &= \sum_{e=1}^{n}\int_{\Omega_e}\frac{1}{2}\sigma\left(\left(\frac{\partial\varphi}{\partial x}\right)^2+\left(\frac{\partial\varphi}{\partial y}\right)^2\right)dxdy \end{aligned} \tag{1}$$

In Equation (1), σ is the conductivity of the triangular unit; φ is the potential function of the triangular unit; Ω is the field area of the grounding grid; Ω_e is the area of the e-th triangular unit; and n is the total number of subdivided units.

Assuming that the current injected into and out of the grounding grid is I, and the nodes correspond to the m and n nodes of the finite element model, the finite element equation is:

$$\begin{bmatrix} K_{11} & K_{12} & \cdots & 0 & \cdots & K_{1N} \\ K_{21} & K_{22} & \cdots & 0 & \cdots & K_{2N} \\ \vdots & \vdots & & \vdots & & \vdots \\ K_{m1} & K_{m2} & \cdots & 0 & \cdots & K_{mN} \\ \vdots & \vdots & & \vdots & & \vdots \\ K_{n1} & K_{n2} & \cdots & 0 & \cdots & K_{nN} \\ \vdots & \vdots & & \vdots & & \vdots \\ K_{l1} & K_{l2} & \cdots & 1 & \cdots & K_{lN} \\ \vdots & \vdots & & \vdots & & \vdots \\ K_{N1} & K_{N2} & \cdots & 0 & \cdots & K_{NN} \end{bmatrix} \begin{bmatrix} \varphi_1 \\ \varphi_2 \\ \vdots \\ \varphi_m \\ \vdots \\ \varphi_n \\ \vdots \\ \varphi_l \\ \vdots \\ \varphi_N \end{bmatrix} = \begin{bmatrix} 0 \\ 0 \\ \vdots \\ I \\ \vdots \\ -I \\ \vdots \\ 0 \\ \vdots \\ 0 \end{bmatrix} \tag{2}$$

Finally, the Gaussian elimination method is used to calculate the node potentials of meshed elements.

2.2. EIT Inverse Problem

EIT sensitive field analysis is an important part of EIT technology [17]. For EIT image reconstruction, its physical model is shown in Equation (3):

$$U = J \cdot \sigma \tag{3}$$

where U is the measurement value of field boundary, σ is the field impedance distribution, and J is the sensitivity matrix response mapping between them.

The purpose of solving the EIT inverse problem is to find out the conductivity distribution of grounding grid conductors that satisfies Equation (4).

$$U(\sigma) = V \tag{4}$$

where $U = [U_1, U_2, U_3 \cdots U_m]^T$ is the calculated voltages, $V = [V_1, V_2, V_3 \cdots V_m]^T$ is the measured voltages, $\sigma = [\sigma_1, \sigma_2, \sigma_3 \cdots \sigma_n]^T$ is the conductivity.

This equation does not hold due to various error factors. The least squares method is used to construct the inverse problem model. It is then transformed into an optimization problem of the objective function, which seeks the conductivity σ that makes $U(\sigma)$ and V as close as possible.

$$\min F(\sigma) = \frac{1}{2} \parallel U(\sigma) - V \parallel_2^2 \tag{5}$$

Equation (5) is a system of nonlinear equations. The true solution can be approximated by iterative solution method.

2.3. Classical Electrical Impedance Imaging Algorithms

In the research of EIT technology, according to the different imaging targets, it can be summarized into two categories: differential imaging and absolute imaging. Differential imaging was studied relatively early; it requires measuring the data at two different time points on the electrodes in the imaging area and then using the imaging algorithm to calculate the difference in the electrical impedance distribution at the two time points for imaging [18]. Absolute imaging takes the absolute value distribution of the imaging area as the imaging target, because absolute imaging reflects the actual distribution of electrical impedance. If a high-resolution reconstructed image can be obtained, its application value will be greatly improved. Because differential imaging does not directly reconstruct the absolute conductivity distribution but is based on the relative change in the reference state, it effectively reduces the complexity of the problem by reducing the range of unknown variables. Therefore, this article is based on differential imaging.

The inverse problem of electrical impedance imaging is actually solving nonlinear equations through the iterative method. Regularization terms are usually added to constrain the objective function to solve the pathology or unsuitability in the inverse problem [19]. Classical image reconstruction algorithms include the truncated regularization algorithm, the Tikhonov regularization algorithm, total variation regularization, the Landweber iterative algorithm, and the Newton-like algorithm [20].

Popular Tikhonov regularization is a further improvement on the least squares algorithm to obtain a more stable generalized inverse algorithm. The constructed generalized function is shown as Equation (6).

$$\min F(\sigma) = \frac{1}{2} \parallel U(\sigma) - V \parallel_2^2 + \frac{1}{2}\alpha \left\| L(\sigma - \sigma^0) \right\|_2^2 \tag{6}$$

where α is the Tikhonov regularization parameter, which is obtained by the L-curve method. L is the regularization matrix, which is taken as the unit array here. σ^0 is the initial conductivity.

Equation (7) is the Gaussian Newton iterative method based on Tikhonov regularization.

$$\sigma^{k+1} = \sigma^{k} - \left(J^T J + \alpha L^T L\right)^{-1} \cdot \left[J^T \left(U\left(\sigma^{k}\right) - V\right) + \alpha L^T L\left(\sigma^{k} - \sigma^{0}\right)\right] \tag{7}$$

where k is the number of iterations, J is the sensitivity matrix, and σ is the conductivity. $U(\sigma)$ is the calculated voltage corresponding to the conductivity under the current iteration.

TV regularization can well maintain the edge characteristics of the image and is very suitable for reconstructing images with sharp edges. When using total variation regularization, the objective function of the inverse problem of electrical impedance tomography is expressed as:

$$\min F(\sigma) = \frac{1}{2}\|U(\sigma) - V\|^2 + \lambda \sum_i |L_i \sigma| \tag{8}$$

where L is a sparse matrix, and $L_i = [0, \cdots, 0, l_i, 0, \cdots, 0]$ where L_i is the length of edge i in the finite element model.

The NOSER is a fast reconstruction algorithm. The algorithm establishes an iterative solution form through the Newton iteration method. The main idea is that when the initial impedance distribution, σ_0, is sufficiently close to the real impedance distribution, σ_t, the number of iterations using the Newton method can be reduced a lot, and even only one step is needed to obtain an approximate impedance distribution result. Because the NOSER is the first step of the Newton algorithm, it has strong real-time performance and is suitable for occasions with high imaging speed requirements.

Using the Newton method for one-step error reconstruction, the solution of the NOSER is:

$$\sigma_{NOSER} = \sigma_0 - \left(J^T J + \alpha L\right)^{-1} J^T (h(\sigma_0) - V) \tag{9}$$

Among them, the regularization matrix $L = diag\left(\sqrt{J^T J}\right)$ is also called the NOSER regularization prior factor.

3. Sparse Representation Theory

In electrical impedance imaging of the grounding grid, reconstruction of impedance images is a typical pathological inverse problem. Traditional reconstruction methods make it difficult to obtain high quality images. To enhance the reconstruction effect, the sparse representation theory is introduced in this article.

3.1. Sparsity

A signal x is sparse if it has a sparse representation under a certain basis or dictionary, that is, the signal can be represented by a linear combination of a small number of non-zero coefficients [21]. Formally, if there exists a basis or dictionary D such that $x = D\alpha$, where α is a sparse coefficient vector (i.e., most of the elements are zero), then it is said to be sparse under the basis D. The schematic diagram of sparse representation is shown in Figure 2.

The sparse representation refers to using a combination of a small number of signals to represent the original signal. This can be regarded as a feature extraction process. These basic signals are called atoms [22]. Given a dictionary $D \subset R^{N \cdot K}$ where K is the number of dictionary columns and N is the number of atoms contained in each column of the matrix. An overcomplete dictionary is an aggregation of atoms whose number exceeds the number of signal dimension, i.e., $N < K$. Using an overcomplete dictionary can effectively extract the features of the signal and make it sparser.

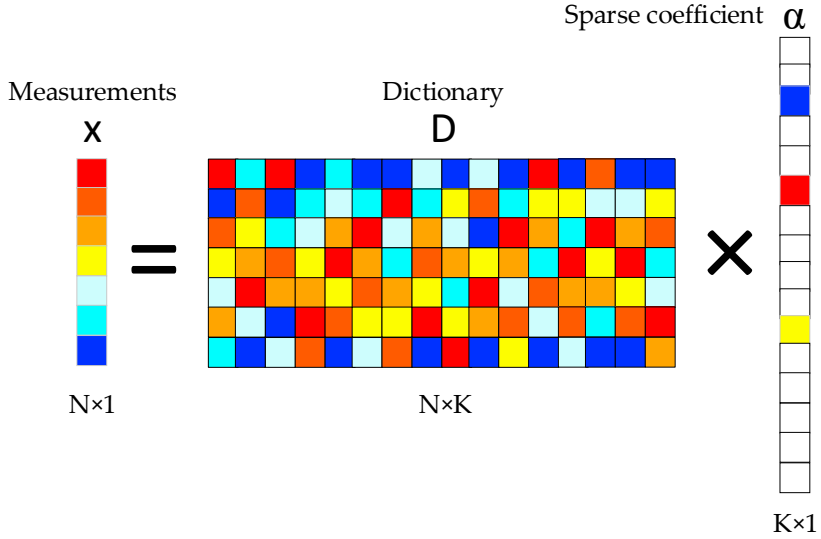

Figure 2. Schematic diagram of sparse representation.

3.2. Sparse Representation Process

The process of sparse representation can be divided into two steps: decomposition and synthesis. Decomposition is the first step in sparse representation, and its goal is to linearly combine the original signal or data through a specific set of bases (or atoms) to form a dictionary. The key in this process is to solve the sparse coefficients required to represent the original signal, that is, the contribution of each basis to the reconstructed signal. Most of these coefficients should be zero or close to zero, with only a few non-zero coefficients [23]. This realizes the sparsity of the signal. Synthesis is the inverse process of sparse representation. The original signal or data are reconstructed using the dictionary and sparse coefficients obtained in the decomposition stage. The original signal can be approximately restored by a linear combination of the bases in the dictionary (each base multiplied by the corresponding sparse coefficient).

4. EIT Reconstruction Algorithm Based on Sparse Representation Theory

Several problems need to be considered when solving the EIT sparse model. First, it is necessary to find a suitable sparse dictionary to ensure effective extraction of feature information and improve sparsity. Second, it is necessary to establish a suitable EIT sparse imaging model. Third, the solution of sparse models often involves complex optimization problems, and it needs to select suitable solution algorithms. Common algorithms include greedy algorithms, convex optimization algorithms, and non-convex optimization algorithms. When selecting an algorithm, it is necessary to consider factors such as convergence, computational complexity, and imaging effect.

4.1. Sparse Representation of Impedance Images

4.1.1. Sparse Representation Model for Impedance Images

In order to enhance the reconstruction effect, soil of the same size as the measurement area is selected as the empty field. The image reconstructed by conductivity is expressed by the difference between empty field conductivity and actual conductivity $\Delta\sigma = \sigma_{empty} - \sigma_{actual}$. This ensures that the data will be as sparse as possible, and then the difference is introduced into the theory of sparse representation. It is obtained by $\Delta\sigma = D\alpha$, which indicates the sparse representation of conductivity difference on a sparse basis D. Thus, the model based on L_1 norms is constructed as follows:

$$\min_{D} \|\Delta\sigma - D\alpha\|_2^2 + \lambda\|\alpha\|_1 \tag{10}$$

where $\Delta\sigma$ is the reconstructed conductivity distribution and λ is the regularization parameter.

4.1.2. Solving for Sparse Coefficients

The sparse representation problem of impedance images requires resolving the sparse coefficients under a given dictionary. Solving the sparse coefficients is a key step in reconstructing the conductivity distribution. There are some methods to solve the sparse coefficients, including the Iterative Shrinkage Thresholding Algorithm (ISTA), the Fast Iterative Shrinkage Thresholding Algorithm (FISTA), Orthogonal Matching Pursuit (OMP), Basis Pursuit (BP), and Least Angle Regression (LARS) [24]. In this article, FISTA is used to solve the sparse coefficients of impedance image.

FISTA is an efficient algorithm for solving sparse optimization problems, especially for optimization problems with L_1 regularization terms. The core principle of the FISTA is to combine ISTA with Nesterov's accelerated gradient technology. It can achieve a fast optimization process, reduce the time complexity of solution, and improve the efficiency of solving large-scale problems. Specifically, FISTA not only relies on the information of current point in each iteration, but also utilizes the information of previous iterations to construct a better update direction, thereby achieving faster convergence.

The specific steps are as follows:

(1) Initialization: initial sparsity coefficient $\alpha(0)$;
Momentum term $y(0) = \alpha(0)$;
Initial acceleration factor $t(0) = 1$;
Setting the step parameter, γ, and the regularization parameter, λ.

(2) Iterative update: In each iteration, the sparsity coefficient, α, the acceleration factor, t, and the momentum term, y, are updated sequentially:

(a) Update the sparsity factor:

$$\min f(x) = ||Ax - y||^2 \tag{11}$$

where $S_{\lambda\gamma}$ is the soft threshold function:

$$S_{\lambda\gamma}(\mathrm{x}) = \mathrm{sign}(\mathrm{x}) \cdot \max(|x| - \lambda\gamma, 0) \tag{12}$$

(b) Update the acceleration factor:

$$t^{(\mathrm{k}+1)} = \frac{1 + \sqrt{1 + 4(\mathrm{t}^{(k)})^2}}{2} \tag{13}$$

(c) Update the momentum term:

$$y^{(\mathrm{k}+1)} = \alpha^{(\mathrm{k}+1)} + \frac{t^{(k)} - 1}{t^{(\mathrm{k}+1)}}(\alpha^{(k+1)} - \alpha^{(k)}) \tag{14}$$

(3) Convergence determination: determine whether the change in α is less than a preset threshold, if so, stop the iteration.

4.2. EIT Sparse Imaging Algorithm

4.2.1. EIT Sparse Imaging Modeling

Based on the sparse expression of the impedance map, an EIT imaging mathematical model is established based on the voltage calculated from the EIT forward problem $U(\sigma)$ and the measured voltage, $V_{measured}$. The model is shown in Equation (11). It is based on the principle of EIT imaging and introduces the theory of sparse expression, which not only makes the imaging outline clearer but also reduces the artifacts that often appear in the reconstructed image and improves the imaging quality.

$$\begin{aligned} &\min \|\Delta\sigma - D\alpha\|_2^2 + \lambda\|\alpha\|_1 \\ &\min \frac{1}{2}\|U(\Delta\sigma) - V_{measured}\|_2^2 \end{aligned} \tag{15}$$

In this article, the Discrete Cosine Transform (DCT) dictionary is chosen as the dictionary for sparse decomposition.

4.2.2. Solution of Sparse Reconstruction Model

The iterative solution of the above model is divided into three main steps:

(1) A DCT dictionary (Discrete Cosine Transform Matrix) is generated based on the finite element profile of the forward problem, initializing the sparse coefficients.
(2) Using the DCT dictionary from the previous step and the sparse coefficients to update the conductivity $\Delta\sigma = D\alpha$, the computed voltage $U(D\alpha)$ is obtained according to Equation (3).
(3) Check if the objective function value Equation (15) is minimized or if the maximum number of iterations has been reached.
(4) Iterate the sparse coefficients according to FISTA mentioned in Section 4.1.2.
(5) Repeat steps 2, 3, and 4. Output $\Delta\sigma$ at the end of the iteration.

5. Imaging Results and Discussions

5.1. Choice of Excitation Mode

The excitation mode of EIT refers to the relative position or mode between electrodes when the excitation signal is injected into the imaging target [17]. These modes have an important impact on the imaging effect and resolution. At present, relative excitation mode and adjacent excitation mode are commonly used in EIT technology. Since the topological structure of the grounding grid is relatively complex, this article chooses the adjacent excitation mode to obtain more data, which is beneficial to image reconstruction. A schematic diagram is shown in Figure 3.

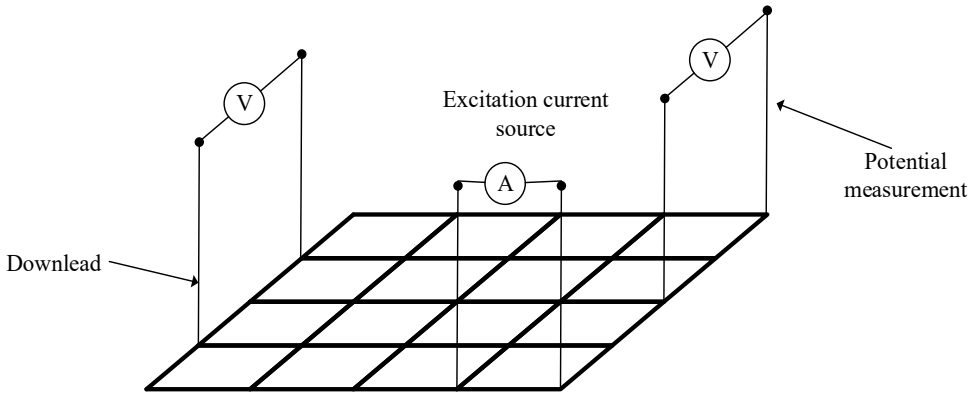

Figure 3. Schematic diagram of adjacent excitation.

Firstly, inject an excitation current of 1 A between two adjacent electrodes, and then the relative potential between other electrodes is measured. Taking the 16-electrode system as an example, the excitation current is first injected between electrode 1 and electrode 2, and the relative potential between the remaining 14 electrodes is measured, with a total of 13 voltage values. Then, the injection electrode is switched to electrode 2 and electrode 3, and the measurement continues. Finally, all adjacent electrode combinations are measured. A total of 208 measurement voltage values are obtained.

5.2. Simulation Modeling in COMSOL

To compare the imaging effect of the algorithm proposed in this article with other algorithms, the COMSOL simulation model of the grounding grid is established to obtain the boundary voltage data, shown as Figure 4. It is a 2 × 2 grounding grid model. A galvanized flat steel with a cross section of 50 mm × 50 mm is built. A square with a side length of 50 cm is constructed. The blue part represents the corroded area. The rest is soil. The conductivity of the uncorroded area is 5.8×10^6 S/m. It is 5.8×10^5 S/m for the corroded area. Conductivity for the soil is set as 5×10^{-3} S/m.

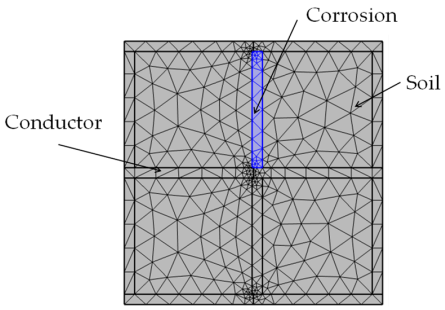

Figure 4. Grounding grid model.

In order to avoid the problem of the true model being exactly the same as the model used to generate the observed data, which would cause inaccurate error estimates, the meshing of the COMSOL model is different from the meshing of the inverse problem in MATLAB, and the COMSOL meshing is coarser.

Then, voltage data can be easily obtained. It is imported into MATLAB for image reconstruction. The finite element meshing of inverse problem model is as shown in Figure 5. There are a total of 3200 small triangles and 1681 nodes.

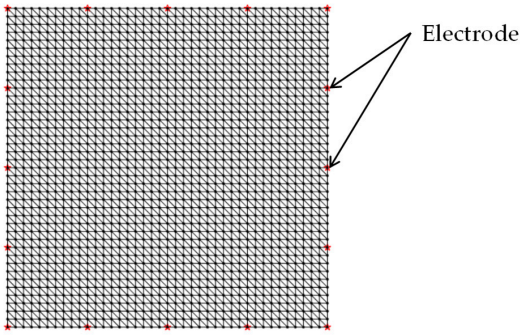

Figure 5. Meshing grid of inverse problem.

5.3. Comparison of Algorithms

The grounding grid model is set up as shown in Figure 4, and the simulated voltage data are obtained by MATLAB in conjunction with COMSOL to compare the Tikhonov regularization algorithm, Total Variation Regularization (TV) algorithm, one-step Newton algorithm (NOSER), and sparse representation imaging Algorithm. The results are shown in Figure 6. Among them, the Tikhonov algorithm and the total variation regularization algorithm (TV) use the L curve method to select the optimal regularization parameter, and the one-step Newton algorithm (NOSER) and the sparse representation imaging algorithm use cross-validation to obtain the optimal regularization parameter. The red part in the reconstructed image indicates the corroded area of grounding grid. This is the same for all subsequent reconstructed images in this paper.

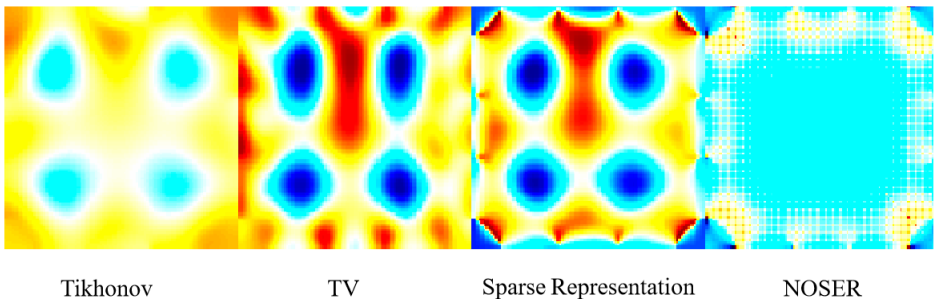

Figure 6. Single branch corrosion imaging.

As can be seen in Figure 6, the quality of reconstructed images under different algorithms varies greatly. The Tikhonov algorithm can image the grounding grid, but only reflects the topology of the grounding grid. The corroded branch is hard to find clearly. The image reconstructed by TV algorithm can clearly reflect the corroded branch and topological structure of the grounding grid. However, there is a "misdiagnosis" on the left side. The NOSER has difficulty in reconstructing the basic outline of the grounding grid in most cases. The sparse representation imaging algorithm can not only clearly see the edge of the grounding grid outline but can also accurately locate and diagnose the corroded branch, greatly reducing "misdiagnoses".

5.4. Multi-Branch Corrosion Diagnosis

The COMSOL simulation is set up with multiple branches corroded, and the reconstructed image is shown in Figure 7. Two branches in red color shows the corroded area for TV and sparse representation algorithm.

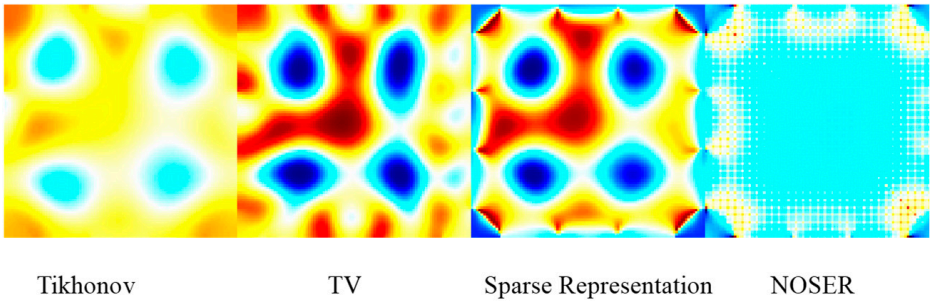

Figure 7. Dual-branch corrosion imaging.

The algorithm proposed in this article for image reconstruction of multiple branch corrosion can still accurately determine the corroded branch, and the misdiagnosis is the least among the above four algorithms.

5.5. Effects of Different Parameters on Imaging Effects

This article uses the L_1 norm to perform sparse representation of the ground grid reconstructed image as the objective function constraint. Usually, the selection of regularization parameters has a huge impact on the solution effect of the algorithm [18].

This article selects the regularization sparsity of sparse representation by generalized cross validation. GCV can select the appropriate regularization parameter according to the characteristics of the data. It does not rely on any prior knowledge of the ideal image, so the generalized cross validation method is selected to select the regularization parameter. The basic form of generalized cross validation can be expressed as:

$$\min GCV(\lambda) = \frac{\|U_\lambda(\Delta\sigma) - V_{measured}\|_2^2}{n \cdot \left(1 - \frac{trace\left(J\left(J^TJ + \lambda I\right)^{-1}J^T\right)}{n}\right)^2} \tag{16}$$

where J is the sensitivity matrix, $U_\lambda(\Delta\sigma)$ is the voltage data obtained by reconstructing the conductivity with the regularization parameter λ, $V_{measured}$ is the measurement data, n is the number of voltage data, and I is the unit matrix.

The model established in this article is shown in Figure 4. Firstly, the optimal regularization parameters were obtained using the generalized cross validation (GCV) method as shown in Figure 8, and image reconstruction was performed at 0.1 times, 0.5 times, 1 time, 1.5 times, and 2 times the optimal regularization coefficients. The results are shown in Figure 9:

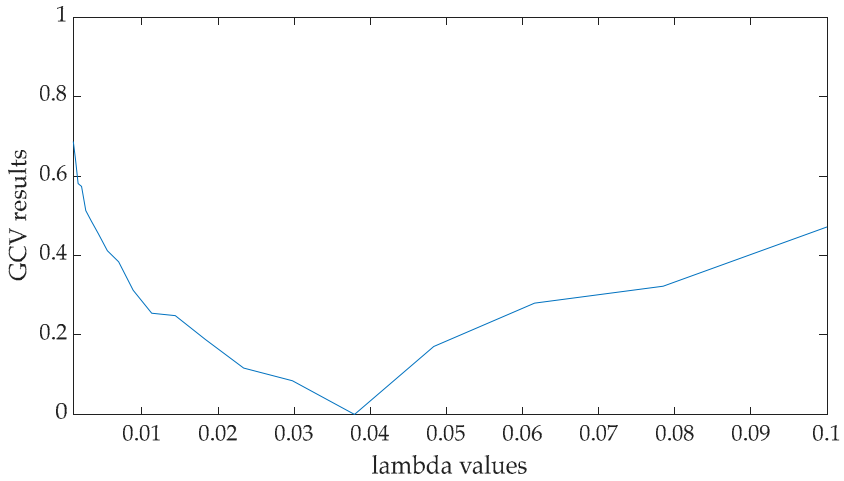

Figure 8. GCV optimization result for regularization parameter.

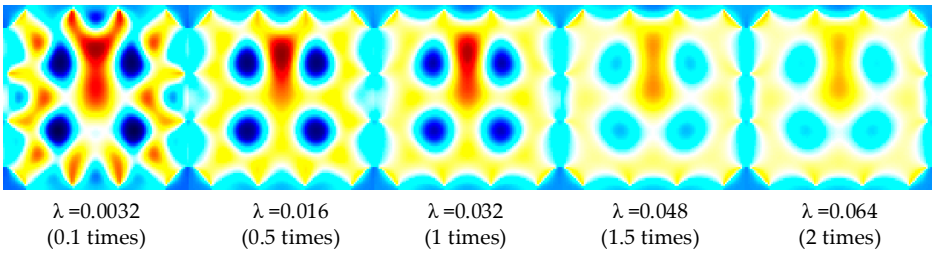

Figure 9. Reconstructed images under different regularization parameters.

It can be seen from Figure 9 that when the regularization parameter is 0.1 times the optimal regularization parameter, the corrosion position of the grounding grid can be seen, but there are some misdiagnoses. When the regularization parameters are 0.5 times, 1 time, and 1.5 times the optimal regularization parameters, the topological structure of the grounding grid can be accurately determined, and the corrosion position can be accurately determined. Therefore, the change in the regularization parameter of this algorithm within a certain range will not affect the imaging effect.

5.6. Noise Impact

In the actual electrical impedance imaging process, voltage data are usually interfered by a certain degree of noise due to factors such as measurement equipment and environmental changes. To model this noise, we assume that the voltage measurement data contain Gaussian noise, with a signal-to-noise ratio (SNR) typically between 20 dB and 40 dB.

In order to evaluate the impact of noise, we conducted simulation experiments at different noise levels. The model is shown in Figure 4, and used Tikhonov regularization algorithm, total variation regularization algorithm (TV), one-step Newton algorithm (NOSER), and Sparse representation imaging algorithm performs reconstruction of conductivity distribution.

Figure 10 is a diagram showing a voltage signal with a Gaussian noise of 20 dB added and a voltage signal without noise, and Figure 11 is a diagram showing the reconstructed image effect with a noise of 20 dB added.

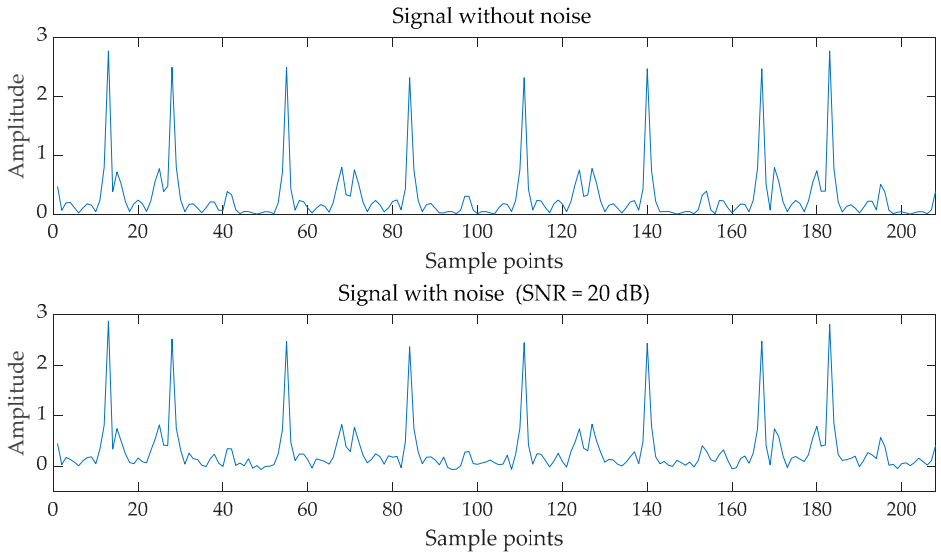

Figure 10. Voltage waveforms without noise and with noise (SNR = 20 dB).

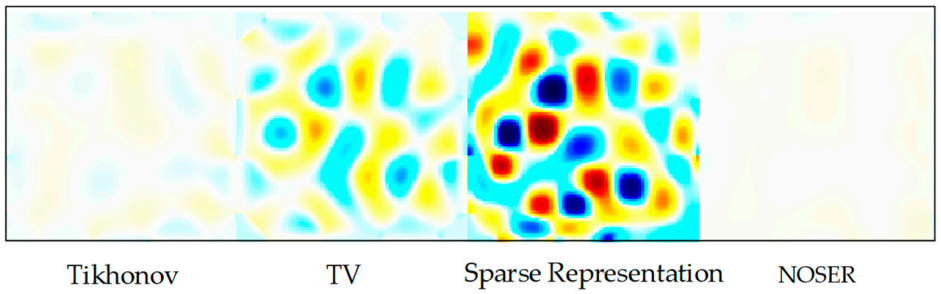

Figure 11. Imaging with noise (SNR = 20 dB).

Figure 12 is a diagram showing a voltage signal with a Gaussian noise of 30 dB added and a voltage signal without noise, and Figure 13 is a diagram showing the reconstructed image effect with a noise of 30 dB added.

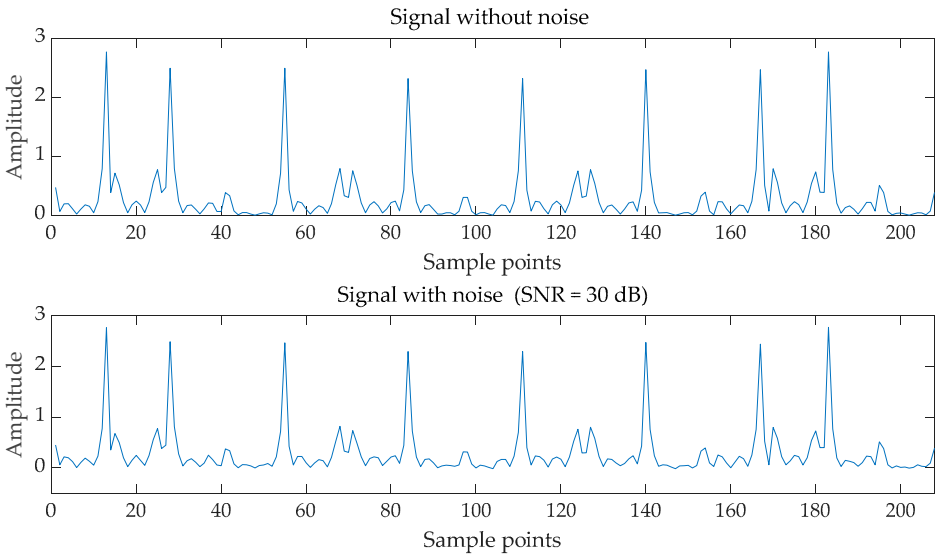

Figure 12. Voltage waveforms without noise and with noise (SNR = 30 dB).

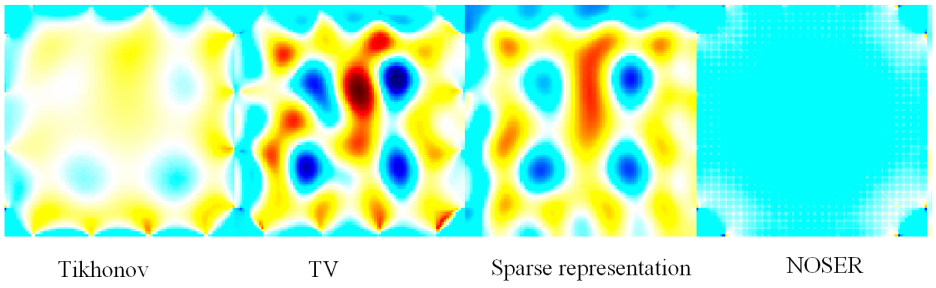

Figure 13. Imaging with noise (SNR = 30 dB).

Experimental results show that when the noise signal-to-noise ratio is lower than 20 dB, the reconstruction results suffer from large deviations, while when the noise signal-to-noise ratio is higher than 30 dB, the sparse representation method can effectively reduce the impact of noise on image reconstruction. Through appropriate regularization, especially sparse representation regularization, the reconstruction quality of images can be significantly improved, especially in high-noise environments.

5.7. Multi-Grid Imaging Analysis

Considering that there is corrosion in one or more branches of the substation grounding grid, and the conductor in the horizontal direction of the grounding grid itself is a simple mesh structure, the distance between each branch is large, and the length of the measuring lead is limited. This article takes a 3×4 grounding grid simulation model and artificially divides it into two parts ($3 \times 3 + 3 \times 1$), uses COMSOL finite element simulation software to obtain boundary potential data, and performs block imaging of the grounding grid, where the corrosion position is marked in red in the figure, and the non-corrosion conductivity is set to 5.8×10^6 S/m and the corrosion area is 5.8×10^5 S/m as shown in Figure 14, to verify the effect of sparse representation imaging algorithm in grounding grid EIT image reconstruction.

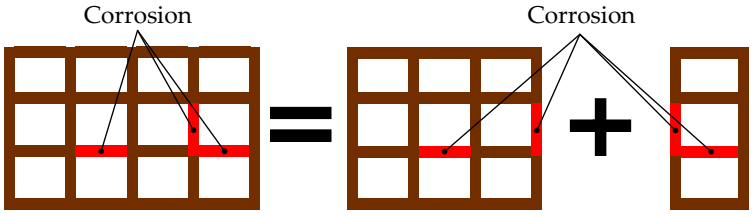

Figure 14. Multi-grid corrosion settings.

The grid is divided into $3 \times 3 + 3 \times 1$, and the voltage is obtained through COMSOL simulation. The image reconstruction results are shown in Figure 15 for 3×3 grid imaging and Figure 16 for 3×1 grid imaging.

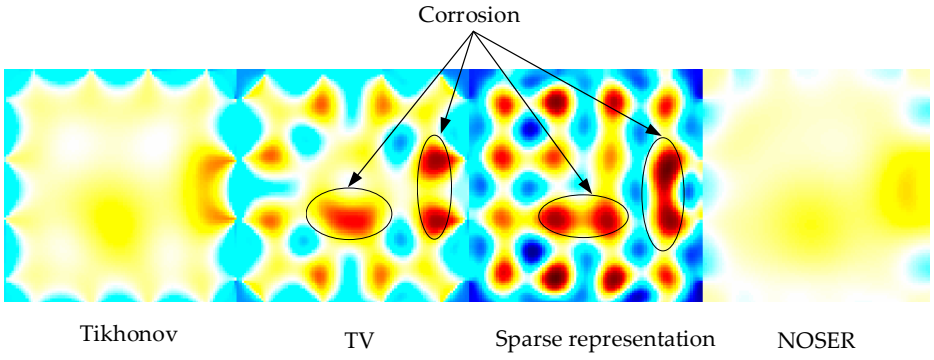

Figure 15. Multi-grid imaging comparison: 3×3 Grid.

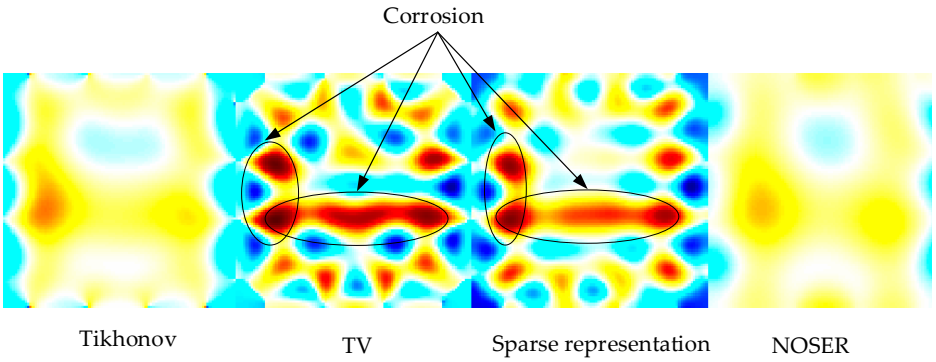

Figure 16. Multi-grid imaging comparison: 3 × 1 Grid.

5.8. Analysis of Multi-Grid Imaging Effects

For the above schemes, it can be seen from the image that the sparse representation imaging effect is still the best, and it can accurately perform visual diagnosis. In order to quantitatively evaluate the reconstructed grounding grid image and to further quantitatively analyze the quality of the grounding grid image based on the sparse representation theory, this article introduces the voltage relative error to evaluate the reconstructed image, which is defined as:

$$EV = \sqrt{\frac{(U(\sigma) - V)^T (U(\sigma) - V)}{V^T V}} \tag{17}$$

According to the optimal regularization parameter, the voltage relative error comparison of the four algorithms is shown in Figure 17.

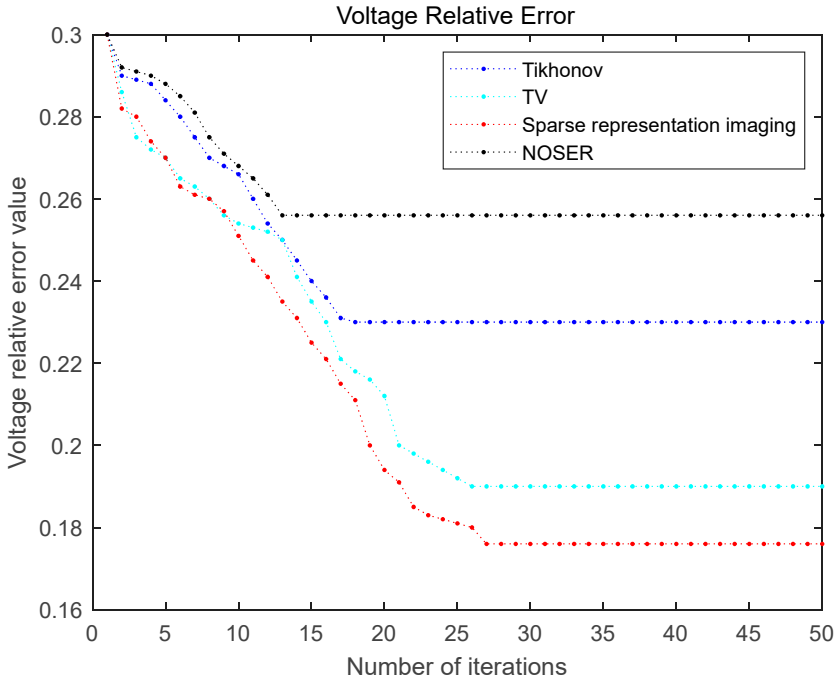

Figure 17. Comparison of voltage relative error.

As shown in Figure 17, no matter what corrosion state the grounding grid is in, the sparse representation algorithm has the highest convergence accuracy. Under the algorithm proposed in this article, the relative error of the grounding grid reconstructed image is reduced by 12.54% on average. This shows that the solution of the grounding grid conductivity under this algorithm is closer to the true value.

6. Conclusions

This article conducts an in-depth study on the ground grid impedance imaging algorithm based on sparse representation and reveals its advantages in reconstructed image quality by comparing it with the Tikhonov algorithm, total variation regularization (TV) algorithm, and one-step Newton (NOSER) algorithm. With significant advantages, multi-grid imaging analysis was performed, and the impact of regularization coefficients on imaging effects was discussed, which is summarized as follows:

(1) The sparse representation imaging algorithm can not only clearly depict the edges of the grounding grid outline and show extremely high image resolution but can also accurately and accurately locate corrosion branches, providing detailed and reliable information for the maintenance and detection of grounding grids.
(2) In contrast, although the Tikhonov algorithm can initially outline the topological structure, it lacks detailed information; the TV algorithm has made progress in corrosion detection, but there is a misdiagnosis phenomenon; with the NOSER, it is difficult to effectively reconstruct the outline of the grounding grid.
(3) The reconstruction algorithm based on sparse representation is superior to other methods in terms of reconstruction error and image quality. It has shown broad application prospects in the field of ground grid electrical impedance imaging and can provide powerful support for technological progress and practical applications in related fields.
(4) Compared with the existing electrical network method, the transient electromagnetic method, and the electrochemical method, the advantage of the grounding grid electrical impedance imaging method based on sparse representation is that it can provide high-resolution corrosion diagnostic images non-invasively and at a low cost and can quickly locate the corrosion area without destroying the grounding grid structure, thus, improving the accuracy and efficiency of diagnosis. Compared with the method based on laser-induced breakdown spectroscopy (LIBS) to measure the corrosion degree of the grounding grid, the method proposed in this article can perform overall imaging in a wider grounding grid area, revealing the overall picture of the corrosion distribution.

In the future, there is a need to better explore regularization methods based on this paper to correct and optimize the mathematical model of the grounding grid EIT inverse problem. At the same time, secondary processing for generated images can be added to accurately diagnose the corrosion location of grounding grid.

Author Contributions: Conceptualization, X.B.; Methodology, Z.X.; Validation, Z.F.; Investigation, D.L.; Data curation, X.B.; Writing—original draft preparation, K.Z.; Writing—review and editing, D.L., Z.F. and Z.X.; Visualization, D.L.; Project administration, K.Z.; All authors have read and agreed to the published version of the manuscript.

Funding: The research was funded by Science and Technology Project of State Grid Sichuan Electric Power Company: Research on online monitoring technology and system development of grounding grid operation status (No. 52199723001M).

Data Availability Statement: The original contributions presented in this study are included in the article. Further inquiries can be directed to the corresponding author.

Conflicts of Interest: The authors declare no conflict of interest.

References

1. Dong, M.; Shi, Z.; Li, X.; Shao, G.; Yang, F.; Yao, D.; Zhang, K. A Diagnosis of Grounding Grid Corrosion Defects Based on Branch Voltage Disturbance. *IEEE Access* **2020**, *8*, 36749–36756. [CrossRef]
2. Hu, H.Z.; Luo, R.C.; Fang, M.G.; Zeng, S.L.; Hu, F.Y. A New Optimization Design for Grounding Grid. *JEPE* **2019**, *108*, 61–71. [CrossRef]
3. Zhang, C.; Liao, Y.; Gao, X.; Zhao, J.; Yuan, Y.; Liao, R. Research Advances of Soil Corrosion of Grounding Grids. *Micromachines* **2021**, *12*, 513. [CrossRef] [PubMed]

4. Yan, X.; Huang, S.; Smolik, W.T.; Chen, W.; Yang, S. A Detection Method for Fast Electrical Impedance Imaging of Grounding Grid Based on Optimized Differential-Multigrid-Homotopy Algorithm. *IEEE TIM* **2023**, *72*, 1. [CrossRef]
5. Huang, Z.; Xia, L.; Zhang, H.; Liu, F.; Tu, Y.; Yang, Z.; Wei, W. Evaluation of Grounding Grid Corrosion Extent Based on Laser-Induced Breakdown Spectroscopy (LIBS) Combined with Machine Learning. *Comput. Electr. Eng.* **2024**, *120*, 109849. [CrossRef]
6. Lu, C.; Li, L.; Liu, Z.; Xu, C.; Xin, M.; Fu, G.; Wang, T.; Wang, X. Location and Corrosion Detection of Tower Grounding Conductors Based on Electromagnetic Measurement. *Measurement* **2022**, *199*, 111469. [CrossRef]
7. Varanasi, S.K.; Manchikatla, C.; Polisetty, V.G.; Jampana, P. Sparse Optimization for Image Reconstruction in Electrical Impedance Tomography. *SIAM Rev.* **2019**, *41*, 85–101. [CrossRef]
8. Cheng, X.; Liu, J.; Zheng, K.; Wu, Z.; Shi, L.; Hu, X. Monitoring of Damage Evolution in Carbon Fiber Reinforced Polymer Composites by Electrical Impedance Tomography. *NDT E Int.* **2024**, *148*, 103239. [CrossRef]
9. Witkowska-Wrobel, A.; Aristovich, K.; Crawford, A.; Perkins, J.D.; Holder, D. Imaging of Focal Seizures with Electrical Impedance Tomography and Depth Electrodes in Real Time. *NeuroImage* **2021**, *234*, 117972. [CrossRef]
10. Gagnon, H.; Grychtol, B.; Adler, A. A Comparison Framework for Temporal Image Reconstructions in Electrical Impedance Tomography. *Physiol. Meas.* **2015**, *36*, 1093–1107. [CrossRef]
11. Keeshan, B.; Adler, A.; Rossa, C. Improved Configurations for 3D Acoustoelectric Tomography with a Minimal Number of Electrodes. *IEEE Trans. Biomed. Eng.* **2023**, *70*, 3501–3512. [CrossRef] [PubMed]
12. Zhong, H.; Sun, B.; Liu, X.; Zhao, X.; Wang, H. Sensitivity-Matrix-Independent Electrical Impedance Tomography: Damage Detection for Composite Materials. *Measurement* **2024**, *236*, 115129. [CrossRef]
13. Jin, B.; Xu, Y.; Yang, J.; Zhang, K. Discontinuous Polynomial Approximation in Electrical Impedance Tomography with Total Variational Regularization. *Commun. Nonlinear Sci.* **2024**, *137*, 108166. [CrossRef]
14. Zamani, M.; Bayford, R.; Demosthenous, A. Adaptive Electrical Impedance Tomography Resolution Enhancement Using Statistically Quantized Projected Image Sub-Bands. *IEEE Access* **2020**, *8*, 99797–99805. [CrossRef]
15. Coxson, A.; Mihov, I.; Wang, Z.; Avramov, V.; Barnes, F.B.; Slizovskiy, S.; Mullan, C.; Timokhin, I.; Sanderson, D.; Kretinin, A.; et al. Machine Learning Enhanced Electrical Impedance Tomography for 2D Materials. *Inverse Probl.* **2022**, *38*, 085007. [CrossRef]
16. Park, J.; Jung, B.G.; Kang, J.W. Nonlinear Electrical Impedance Tomography Method Using a Complete Electrode Model for the Characterization of Heterogeneous Domains. *CMES* **2023**, *134*, 1707–1735. [CrossRef]
17. Yoon, S.; Kim, M.K.; Kim, T.U.; Jeon, D.; Song, H.; Suh, J.-I.; Oh, J.E.; Kim, D.J. Enhancing Image Resolution in Single-Side Electrical Resistance Tomography (ERT) by Utilizing Theoretical Sensitivity Analysis: Experimental Validation and Application to Cement Mortar. *JOBE* **2024**, *84*, 108480. [CrossRef]
18. Liu, D.; Smyl, D.; Du, J. A Parametric Level Set-Based Approach to Difference Imaging in Electrical Impedance Tomography. *IEEE TMI* **2019**, *38*, 145–155. [CrossRef] [PubMed]
19. Nguyen, D.M.; Andersen, T.; Qian, P.; Barry, T.; McEwan, A.L. Electrical Impedance Tomography for Monitoring Cardiac Radiofrequency Ablation: A Scoping Review of an Emerging Technology. *Med. Eng. Phys.* **2020**, *84*, 36–50. [CrossRef] [PubMed]
20. Wang, Z.; Liu, X. A Regularization Structure Based on Novel Iterative Penalty Term for Electrical Impedance Tomography. *Measurement* **2023**, *209*, 112472. [CrossRef]
21. Akhavan, S.; Baghestani, F.; Kazemi, P.; Karami, A.; Soltanian-zadeh, H. Dictionary Learning for Sparse Representation of Signals with Hidden Markov Model Dependency. *Digit. Signal Process.* **2022**, *123*, 103420. [CrossRef]
22. Lin, Z.; Jia, S.; Zhou, X.; Zhang, H.; Wang, L.; Li, G.; Wang, Z. Digital Holographic Microscopy Phase Noise Reduction Based on an Over-Complete Chunked Discrete Cosine Transform Sparse Dictionary. *Opt. Laser Eng.* **2023**, *166*, 107571. [CrossRef]
23. Wang, X.Y.; Li, X.P.; So, H.C. Robust Sparse Representation Based on Fitting Error Decomposition. *Signal Process.* **2024**, *222*, 109523. [CrossRef]
24. Xiao, P.; Qiu, P.; Ha, S.; Bani, A.; Zhou, S.; Sotiras, A. SC-VAE: Sparse Coding-Based Variational Autoencoder with Learned ISTA. *Pattern Recognit.* **2024**, *161*, 111187. [CrossRef]

Disclaimer/Publisher's Note: The statements, opinions and data contained in all publications are solely those of the individual author(s) and contributor(s) and not of MDPI and/or the editor(s). MDPI and/or the editor(s) disclaim responsibility for any injury to people or property resulting from any ideas, methods, instructions or products referred to in the content.